Supporting information for
Bandwidth limitation of directly contacted graphene-silicon optoelectronics

Dun Mao[1], *Thomas Kananen*[1], *Tiantian Li*[1], *Anishkumar Soman*[1], *Jeffrey Sinsky*[2], *Nicholas Petrone*[3], *James Hone*[3], *Po Dong*[2], *Tingyi Gu*[1*]

[1]Department of Electrical and Computer Engineering, University of Delaware, Newark, Delaware 19716, USA

[2]Nokia Bell Labs, 791 Holmdel Road, Holmdel, New Jersey 07733, USA

[3]Department of Mechanical Engineering, Columbia University, New York, NY 10027

*E-mail: tingyigu@udel.edu

S1. S_{11} Curve fitting results for the small-signal model

The figures below are measured S_{11} under forward bias. It can be seen from the figure that for the Si *p*-*i*-*n* junction, as the bias increases, the S_{11} magnitude and phase rarely change throughout the frequency range. For the G-Si *p*-*i*-*n* junction, S_{11} magnitude goes down while the phase varies little with an increased bias.

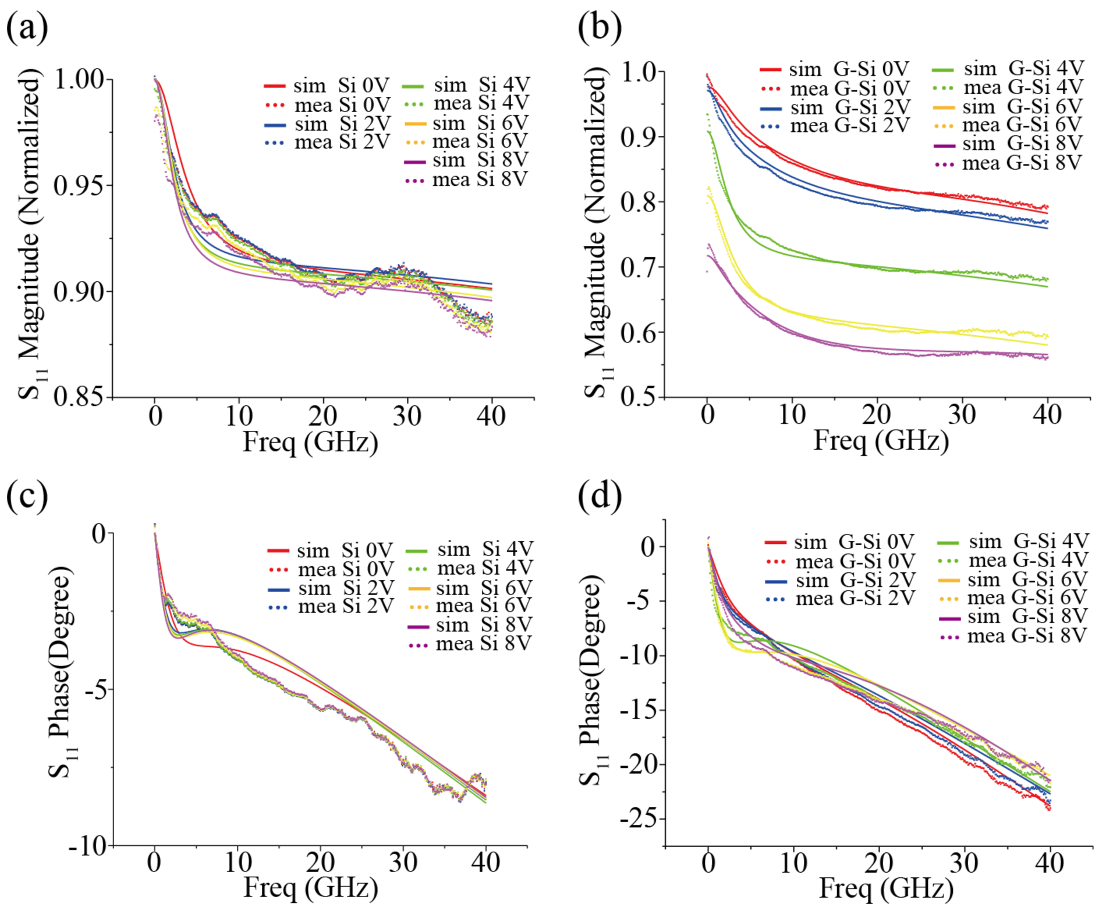

Figure S1. Measured and simulated S_{11} for Si and G-Si *p-i-n* junction under 0 V, 2 V, 4 V, 6 V and 8 V bias: (a) magnitude of Si, (b) magnitude of G-Si, (c) phase of Si; (d) phase of G-Si *p-i-n* junction.

Advance system design (from Keysight) is used for the curve fitting. Standard error is utilized for the error bar as the reference. Measured S parameter (S_{11}) is set as the optimization goal, and parameters are optimized to fit simulated S_{11} towards measured S_{11}. The error can be represented as:

$$e11(V) = \frac{\sqrt{\sum_i^N \left|S_{11,\text{fitted}}(fi,V) - S_{11,\text{measured}}(fi,V)\right|^2}}{\sqrt{N}}$$

Where fi is the i^{th} frequency point, N is the total number of frequency points in the frequency range and V stands for each bias.

Global optimization was used for circuit elements fitting under every bias during the simulation process. For the simulated circuit elements (R, L, C) under each bias, they may not be the only values, but they serve to achieve the smallest standard error referring to the optimization goal. It can be seen from Session S3 in this supporting information file that the fitting results seem to be reasonable and consistent for the range and scale.

S2. Simulated built-in electric field components E_x, E_z at hybrid junction interface (xz cross-sectional plane) of G and Si *n* region under bias of 0 V, 2 V, 4 V, 6 V, 8 V

Figure S2 shows that the simulated built-in electric field components, E_x and E_z, increase around the G and Si *n*-region interface as the bias increases.

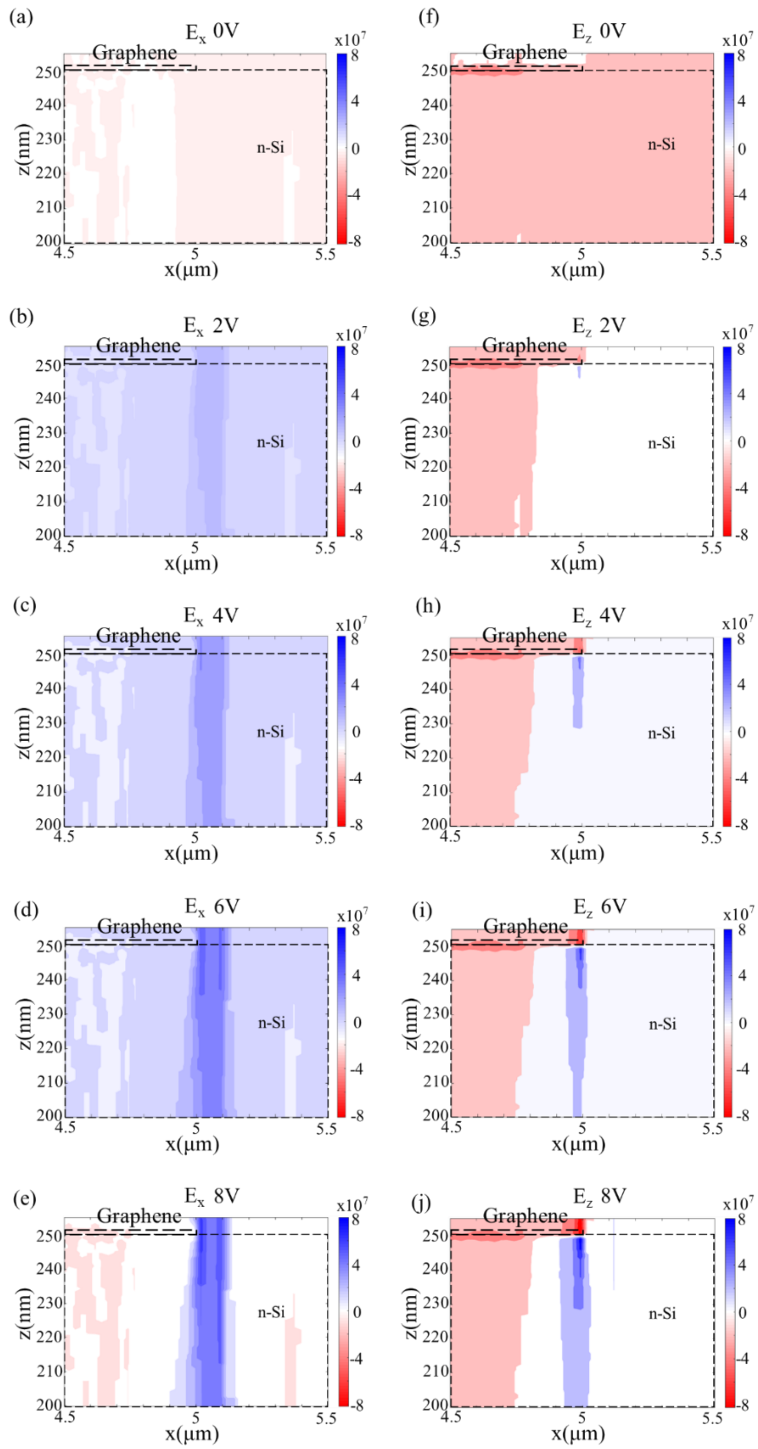

Figure S2. Simulated built-in electric field components at hybrid junction interface of G and Si *n* region varying with bias: (a~e) E_x under bias of 0 V, 2 V, 4 V, 6 V, 8 V; (f~j) E_z under bias of 0 V, 2 V, 4 V, 6 V, 8 V.

S3. Estimation of graphene inductance, resistance

In order to verify the fitting results of small signal model, estimation of graphene inductance and resistance is essential for reference.

Researchers have studied on-graphene kinetic inductance based on graphene model as a transmission line. The kinetic inductance is as following[S1]:

$$L_k W = \frac{\pi\hbar}{e^2 v_F} \times \frac{1}{\sqrt{n_0}}$$

Where the parameters showing on the equation can be seen from the following table:

Table S1. Parameters used for calculating graphene inductance.

	Description	Value
$\boldsymbol{v_F}$	Fermi velocity	$10^6\ m/s$
$\boldsymbol{e}$	Electric charge	$1.6\times 10^{-19}\ C$
$\hbar$	Reduced Planck's constant	$1.0545718 \times 10^{-34}\ J \cdot s/rad$
$\boldsymbol{n_0}$	Carrier density	$10^{10}\sim 10^{14} cm^{-2}$
$\boldsymbol{W}$	Width of graphene	$2.5\ \mu m$
$\boldsymbol{L_k}$	Kinetic inductance of graphene per unit length	

Here we estimate a range for the carrier density to be 10^{10} to 10^{14} cm^{-2}, and plot it using Matlab:

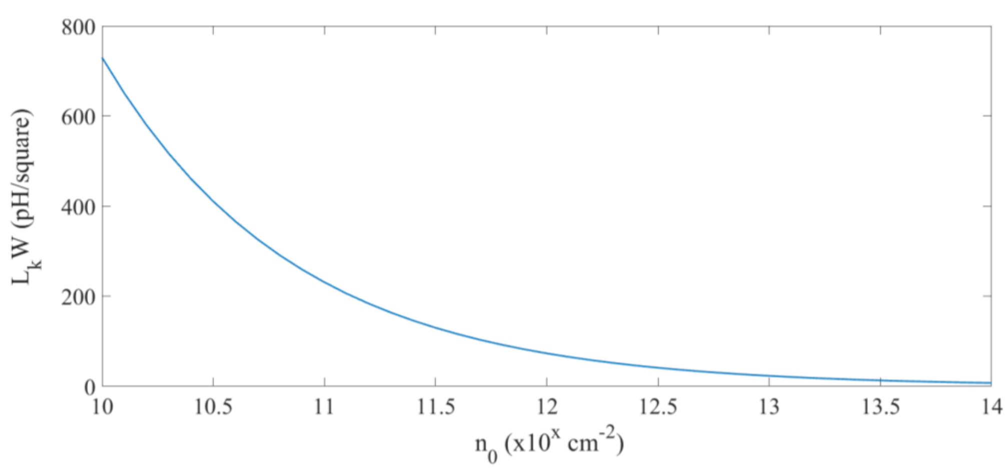

Figure S3. Calculated graphene inductance varying with carrier density.

As shown in Figure S3, the graphene inductance ranges from 7.301~730.1 pH per square as density varies from 10^{10}~10^{14} cm^{-2}. In Figure 5(a) of the main text, extracted graphene inductance after curve fitting ranges approximately from 8~24 pH which is corresponding to the carrier density from 8.31~0.93×10^{13} cm^{-2} referring to Figure S3.

For the graphene resistance, calculated results are compared with the fitting results in the main text.

Resistance is defined as following:

$$R = \frac{\rho l}{A}$$

Resistivity ρ has the relationship with conductivity σ:

$$\rho = \frac{1}{\sigma}$$

Relationship between conductivity σ, mobility μ, mean free path l_c is shown as: [S2]

$$\sigma = en\mu = \frac{2e^2(k_F l_c)}{h}$$

where

$$k_F = (\pi n)^{\frac{1}{2}}$$

The resistance of graphene can be written as the following:

$$R = \frac{\rho l}{A} = \frac{l}{\sigma A} = \frac{h \cdot l}{2e^2(k_F l_c)A} = \frac{h \cdot l}{2e^2((\pi n)^{1/2} l_c)A}$$

Based on the equation above, for our device, parameter values of graphene resistance can be noted in the following table:

Table S2. Parameters used for calculating graphene resistance.

	Description	Value
$\boldsymbol{h}$	Planck's constant	$6.626 \times 10^{-34}\ J \cdot s$
$\boldsymbol{l}$	length	$2.5\ \mu m$
$\boldsymbol{e}$	Electric charge	$1.6 \times 10^{-19}\ C$
$\boldsymbol{l_c}$	Mean free path	$3.5\ \mu m$
$\boldsymbol{A}$	Area of graphene	$3\ \mu m$
$\boldsymbol{n_0}$	Carrier density	$10^{10} \sim 10^{14}/cm^2$

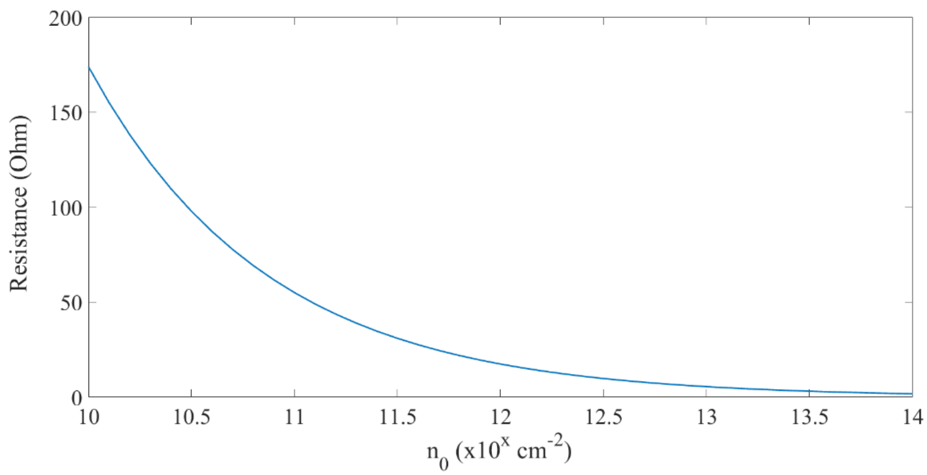

Figure S4. Plot of graphene resistance varying with carrier density.

Figure S4 shows based on calculated results, that the graphene resistance ranges from 1.7~173.8 Ohm as the carrier density varies from 10^{10}~10^{14} cm^{-2}. In Figure 5(b) in the main text, extracted graphene resistance after curve fitting ranges approximately from 2~6 Ohm which corresponds to the carrier density 7.58~0.83×10^{13} cm^{-2} referring to Figure S4. The estimated carrier density based on graphene resistance is very close to the estimated carrier density based on graphene inductance. These results show the consistency and reasonableness for the carrier density estimation based on the fitting results.

S4. Bias dependent junction parameters

The figures below are the remaining circuit element variations under different biases. For junction resistances R_{pi} and R_{in}, junction capacitances C_{pi} and C_{in}, capacitance C_1, resistances R_1 and R_2, they all vary significantly as the bias increases, while resistances R_3 and R_5 don't fluctuate remarkably.

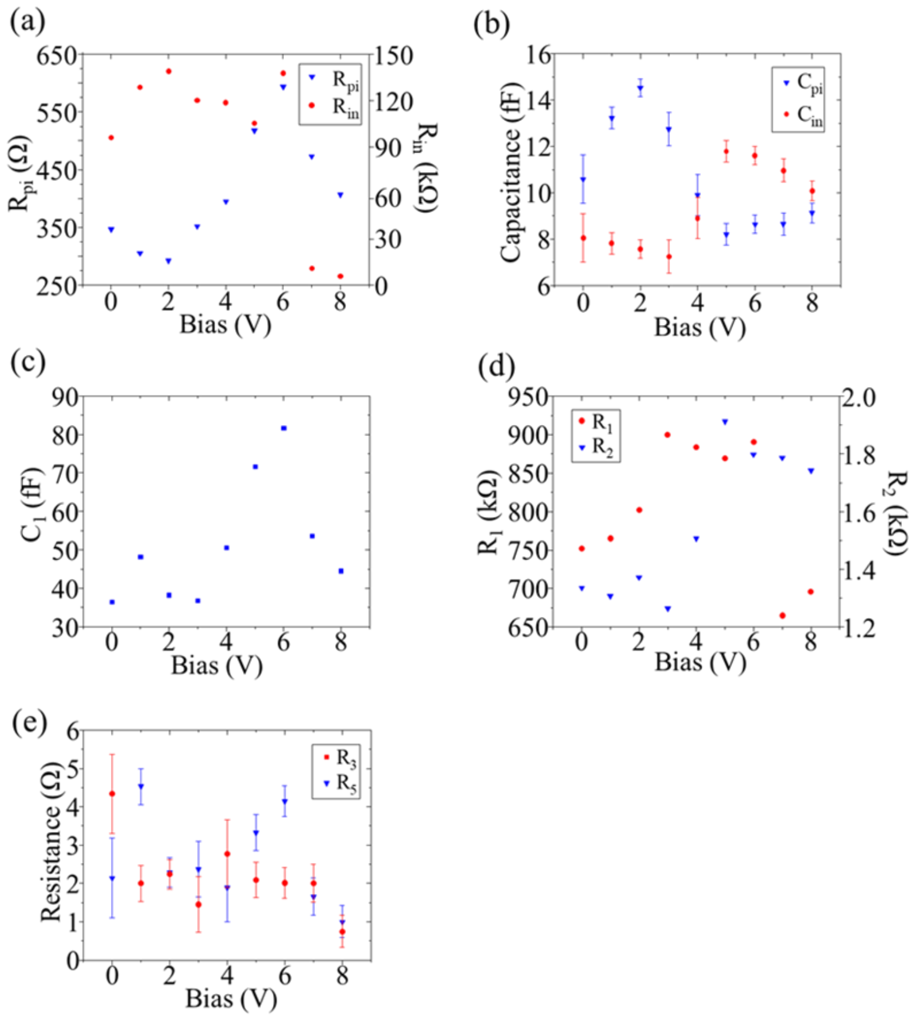

Figure S5. Remaining extracted circuit elements varying the bias from 0 V to 8 V for Si and G-Si *p-i-n* junction: (a) junction resistances R_{pi}, R_{in}; (b) junction resistances C_{pi}, C_{in}; (c) silicon oxide capacitance C_1; (d) resistances R_1, R_2; (e) resistances R_3, R_5. Error bar indicates standard errors of the mean for extracted parameters. For R_{pi}, R_{in}, C_1, R_1, and R_2, the errors are very small compared to their values and can be neglected – thus not shown in the figures.

S5. Summary of G based Photodetectors and modulators

Selected research tasks involving graphene photodetectors are shown in the Figure S6 (a) for comparison. Graphene metal heterojunction photodetectors have been demonstrated which can achieve over 100 GHz but with very low Signal-to-Noise Ratio (SNR) less than 1 dB,[S6] or attain 25 dB SNR and over 70 GHz bandwidth.[S5] Other works using graphene silicon directly contacted photodetectors have SNR less than 15 dB and very low bandwidth.[S8-9] Graphene integrated on a slot waveguide to create a *p-n* junction is demonstrated with 65 GHz bandwidth but SNR is still not very high.[S7] Comparing with other types of graphene-based photodetector, our work of G directly contacted Si *p-i-n* junction based on G absorption not only offers very high SNR over 50 dB but provides bandwidth over 60 GHz as well. For High speed Graphene-based modulators have been investigated by other researchers these years. [S10-20] Different types of modulators based on Si only and G and Si can be seen in Figure S6 (b). For modulators based on Si–insulator–Si capacitor, or travelling wave Mach–Zehnder interferometer lateral Si p-n junction, the bit rate and extinction ratio in the performance matrix cannot be achieved very high simultaneously. [S10-14] Graphene-based modulators can achieve high bit rate or extinction ratio. [S15-19] We believe G Si *p-i-n* modulator based on Graphene absorption will have high bit rate at high extinction ratio and will work on that in future.

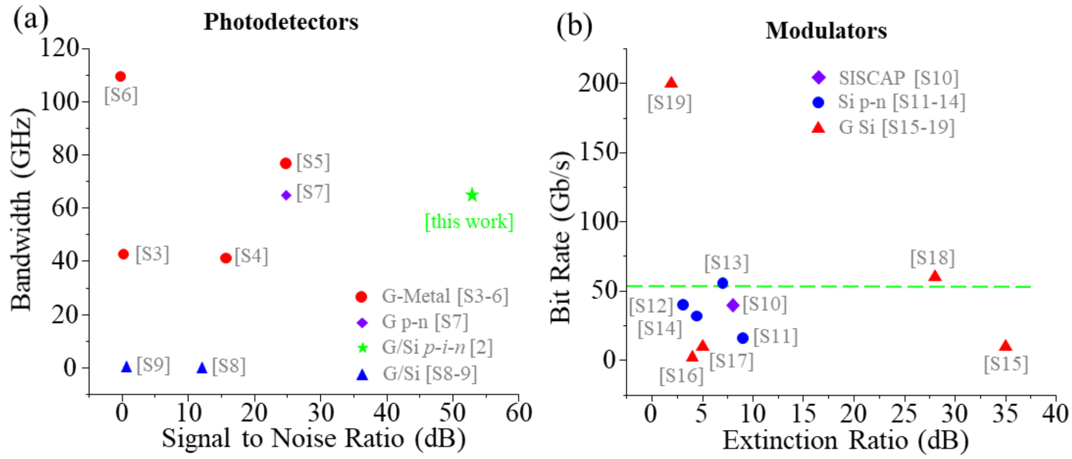

Figure S6: (a) Comparison of the optoelectronic bandwidth and signal-to-noise ratio of G-based photodetectors, (b) comparison of bit rate and extinction ratio of Si and G modulators.

REFERENCES

(S1) Yoon, H.; Forsythe, C.; Wang, L.; Tombros, N.; Watanabe, K.; Taniguchi, T.; Hone, J.; Kim, P.; Ham, D., Measurement of Collective Dynamical Mass of Dirac Fermions in Graphene, *Nature Nanotechnology* **2014**, *9*, 594–599

(S2) Bolotin, K.I.; Sikes K.J.; Jiang, Z.; Klima, M.; Fudenberg, G.; Hone, J.; Kim, P.; Stormer, H.L.; Ultrahigh Electron Mobility in Suspended Graphene, *Solid State Communications* **2008**, *146*, 351-355

(S3) Shiue, R., et al, "High-Responsivity Graphene−Boron Nitride Photodetector and Autocorrelator in a Silicon Photonic Integrated Circuit." *Nano Letter* **2015**, *15*, 7288−7293

(S4) Schall, D., et al, "50 GBit/s Photodetectors Based on Wafer-Scale Graphene for Integrated Silicon Photonic Communication Systems." *ACS Photonics* **2014**, *1*, 781–784.

(S5) Schall, D., et al, "Graphene Photodetectors with a Bandwidth >76 GHz Fabricated in a 6″ Wafer Process Line.", *Journal of Physics D: Applied Physics* **2017**, *50*, 124004.

(S6) Ma, P., et al, "Plasmonically Enhanced Graphene Photodetector Featuring 100 Gbit/s Data Reception, High Responsivity, and Compact Size." *ACS Photonics* **2018**, DOI: 10.1021/acsphotonics.8b01234.

(S7) Schuler, S. et al. "Controlled Generation of a p-n Junction in a Waveguide Integrated Graphene Photodetector. " *Nano Letter* **2016** *16*, 7107–7112.

(S8) Wang, X., et al. "High-Responsivity Graphene/Silicon-Heterostructure Waveguide Photodetectors." *Nature Photonics* **2013**. 7, 888–891.

(S9) An, X., et al. “Tunable Graphene-Silicon Heterojunctions for Ultrasensitive Photodetection”. *Nano Letter* **2013** 13, 909–916.

(S10) Webster, M. A. et al. "Low- Power MOS- Capacitor Based Silicon Photonic Modulators and CMOS Drivers." *Optical Fiber Communication Conference*. **2015** https://doi.org/10.1364/OFC.2015.W4H.3.

(S11) Gill, D. M. et al. "Demonstration of A High Extinction Ratio Monolithic CMOS Integrated Nanophotonic Transmitter and 16 Gb/s Optical Link." *IEEE Journal of Selected Topics in Quantum Electronics* **2015**, *21*, 3400311.

(S12) Ding, R. et al. "Design and Characterization of A 30-GHz Bandwidth Low- Power Silicon Traveling-Wave Modulator." *Optics Communications* **2014**, *321*, 124–133.

(S13) Yang, Y. et al. "High-Efficiency Si Optical Modulator Using Cu Travelling- Wave Electrode." *Optics Express* **2014**, *22*, 29978–29985.

(S14) Gill, D. M. et al. "Demonstration of Error-Free 32 Gb/s Operation from Monolithic CMOS Nanophotonic Transmitters." *IEEE Photonics Technology Letter* **2016**, *28*, 1410–1413.

(S15) Sorianello, V. et al, "Graphene–Silicon Phase Modulators with Gigahertz Bandwidth," *Nature Photonics* **2018**, *12*, 40–44

(S16) Liu, M. et al, "A Graphene-Based Broadband Optical Modulator," *Nature*, **2011**, *474*, 64–67

(S17) Hu, Y. et al, "Broadband 10 Gb/s Operation of Graphene Electro-Absorption Modulator On Silicon," *Laser Photonics Review* **2016**, *10*, 307–316

(S18) Christopher, P. et al, "Graphene Electro-Optic Modulator with 30 GHz Bandwidth," *Nature Photonics* **2015**, *9*, 511–515

(S19) Li, W. et al, "Ultrafast All-Optical Graphene Modulator," *Nano Letter*, **2014**, *14 (2)*, 955–959.

(S20) Romagnoli, M. et al, "Graphene-Based Integrated Photonics for Next-Generation Datacom and Telecom," Nature Reviews Materials, 2018, 3, 392–414.